Supporting Material

Molecular Dynamics Simulations of the Cx26 Hemichannel: Insights into voltage-dependent loop-gating.

Taekyung Kwon, Benoît Roux, Sunhwan Jo, Jeffery B. Klauda, Andrew L. Harris and Thaddeus A. Bargiello

1. Completion of crystal structure and construction of the simulation system.

The atomic coordinates of Met1, all residues in the cytoplasmic loop (CL), the C-terminal domain (CT), the side chains of residues K15, S17, and S19 and all hydrogen atoms were not defined in the published structure of Cx26 (PDB:2ZW3) (1). We completed the structure in the following manner: 1) The coordinates of Met1 were taken from the lowest energy conformer of a N-terminal Cx26 peptide solved by NMR (2). 2) The 15 residue CL segment, which has a high probability of disordered structure, ranging from 0.67 to 0.78 as assessed by metaPrDos (http://prdos.hgc.jp/meta/) (3), was added as a random structure connecting the defined helical portions of TM2 with TM3. The C_α-coordinates of the 15 residue CL were initially assigned by linear interpolation of the distance between residues 109 (TM2) and 125 (TM3). 3) Similarly, metaPrDos predicted that the 9 residue intracellular CT would adopt a random structure and the 9 residues of the CT were built as a linear extension of the TM4 helix. 4) Subsequently, the coordinates of undefined atoms in the CL and CT sequences, and those of residues K15, S17, S19 in the N-terminus were designated by their CHARMM 22 all-atom protein parameters (4, 5). 5) Disulfide bonds identified in the crystal structure were created between C53-C180, C60- C174, and C64-C169 in each of the six subunits. 6) Protonation of histidine residues were determined by the hydrogen bond pattern in the crystal structure and assigned as either HSD or HSE. These assignments agree with the pKa's predicted with PROPKA 3.0, http://propka.ki.ku.dk/ (6-8). 7) The original coordinates of the atoms in the x-ray structure were fixed and the completed structure including all hydrogen atoms was minimized in vacuum using alternate cycles of steepest descent (SD) and adopted basis Newton-Raphson (ABNR) until the energy difference between steps was less than 10^{-7} kcal/mol (3570 SD and 800,000 ABNR total steps). The channel was then integrated into a 1-palmytoyl-2-oleoyl-*sn*-glycero-3-phosphatidylcholine (POPC) lipid membrane. The dimension of the POPC membrane, 150 Å x 150 Å, was twice that of the x-y dimension of the protein. The area of the membrane was determined based on the experimentally determined surface area of a POPC molecule (9) and fixed throughout the simulation. A tetragonal periodic boundary box, 150 Å x 150 Å x 110 Å including the protein, lipid membrane, TIP3 waters, and 150 mM KCl was constructed with Membrane Builder program in CHARMM-GUI (10-12).

2. Molecular dynamics simulations.

All protein atoms in this system used the CHARMM 22 all-atom force field with dihedral cross-term correlation (CMAP) corrections (4, 13). The CHARMM 27r all-atom force field was used for lipid molecules (14). The system was initially equilibrated for 375 ps in CHARMM (15, 16) at 303.15 K, using a method developed by Woolf and Roux (17, 18). Force constraints were reduced, first with NVT dynamics using the Langevin temperature control and then with NP_nAT dynamics using the Nosé-Hoover thermostat (19). The system was equilibrated for 140 ns at 310 K using NP_nAT dynamics in NAMD2.7b2 (20) with no constraints. NVT is the ensemble name for constant number of particles (N), volume (V), and temperature (T). NP_nAT is the ensemble name for constant number of particles (N), pressure in normal direction (P_n), cross-sectional area (A), and temperature (T). Trajectories were calculated with a 2 fs time step (except the initial 75 ps where they were

calculated with a 1 fs time step) with the SHAKE algorithm at 1 atm and 310 K. Electrostatic interactions were calculated using particle mesh Ewald method (PME) (21). Following a 150 ns equilibration, an autocorrelation analysis was performed on the last 10 ns of the RMSD trajectory of the protein, and estimated the relaxation time of the protein backbone as ~2 ns. Based on the relaxation time, four independent 20-ns production stage simulations were performed from the 140 ns time point. The V43A+I74V mutation was created with the IC module of CHARMM on the wild-type structure corresponding to the 140 ns time point. The side chains of the mutated residues were minimized by 200 SD and 200 ABNR steps in CHARMM and equilibrated with an additional 10-ns simulation in NAMD. Autocorrelation analysis of the mutant RMSD provided a relaxation time similar to wild type (~ 2 ns). The trajectories of all van der Waals interactions equilibrated within 10 ps. Consequently, 4 independent 10-ns simulations were performed on the double mutant.

3. Construction of interaction lists.

The van der Waals interaction list was prepared by identifying all atom-atom pairs in the side chains of hydrophobic residues (Ala, Val, Leu, Ile, Met, Phe, Trp and Tyr) that were located within 3 Å of each other for at least 0.2 ns in any of the four replicate 20 ns production stage simulations (1% of the length of the trajectory). The assembled list was converted into a residue-residue list. Time series of distance and van der Waals energies for residue pairs having more than 5 atom-atom interactions were constructed. Residue pairs with interaction energies > -0.3 kcal/mol were not included in the van der Waals interaction list.

The electrostatic interaction list was prepared by identifying all atoms that could participate in hydrogen bond formation that were located within 2.4 Å of each other for at least 0.2 ns in any of the four 20 ns production stage simulations.

Comparison of the electrostatic and van der Waals interaction lists for the crystal and equilibrated Cx26 hemichannels are presented in the Supplement of Kwon et al. (22).

4. Calculation of van der Waals and electrostatic interactions.

van der Waals interactions for pairs of amino acid residues were determined by solutions of Lennard-Jones potentials in CHARMM. For the crystal structure, hydrogen atoms were added with the HBUILD module of CHARMM and their positions minimized as described in the construction of the simulation system. Electrostatic interactions were calculated by solution of Coulombs law in CHARMM.

5. Comparison of electrostatic networks in the crystal and equilibrated structures.

The electrostatic network of the crystal structure, based on our analysis of the atomic coordinates provided in PDB file, 2ZW3, is shown in Fig. 3C and D. The principle difference is the expansion of the electrostatic network following MD simulations to include residues E42 (E1), K188 (TM4), Q48 (E2), N62 and S183 (E2). The participation of both the side chain and backbone carbonyl of E42 in the electrostatic network was absent in the crystal structure, as was the interaction between D46 and K188. In addition we did not observe several interactions proposed by Maeda et al (1). These include hydrogen bonding of R184 ← Y65 as well as Q48 ← D50, and Q48 ← E46. The distance separating R184 and Y65 as well as Q48 and E46 in the dynamic structures fluctuated between 4 and 10 Å, distances much greater than the 2.4 Å (the distance between a proton and it acceptor) required for hydrogen bond formation. The distance between R184 and Y65 and between Q48 and E46 in the crystal structure also exceeds the 2.4 Å cutoff we employ to identify hydrogen bond formation.

Unlike all other charged residues in the TM1/E1 region, K41 is freely mobile in the channel pore and does not participate in any substantial long-lived electrostatic interactions.

6. Figure S1. Fluctuations in backbone H-bonding in the parahelical region. The time series of five H-bonds (green lines in A) that define a parahelix (23) are shown for a representative subunit in the Cx26 hemichannel during the production stage equilibrations. Blue dots in B-F (leftmost sections) are the distances between designated interactions in the crystal structure. We assume H-bonds are formed when the distance between a proton and its acceptor is ≤ 2.4 Å (24).

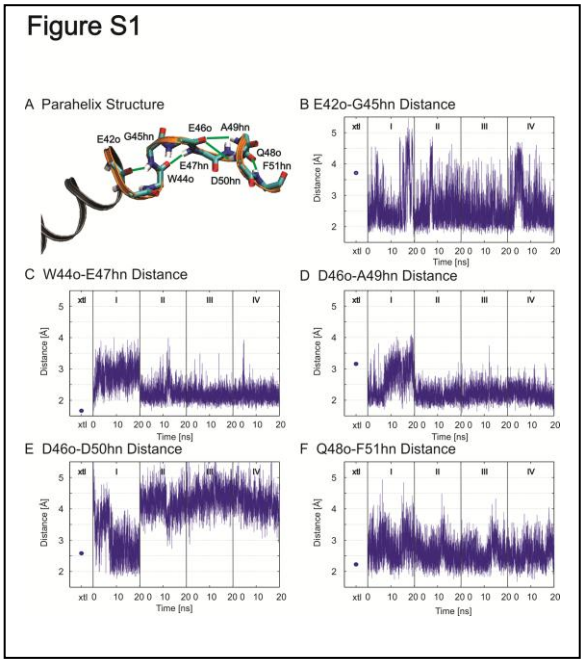

7. Figure S2. Stabilization of the TM1/E1 bend angle. In addition to the A39o – V43hn hydrogen bond (depicted by dashed green lines and labeled (1) and van der Waals interactions (Fig. 2), the TM1/E1 bend angle is stabilized by electrostatic interactions between K22 (TM1) and E209 (TM4) (labeled (2)) and R32 (TM1) and E147 (TM3) (labeled (3). Arrow indicates TM1/E1 bend angle. Fluctuations in the time series of both electrostatic interactions shown in panels B and C are representative of all six subunits.

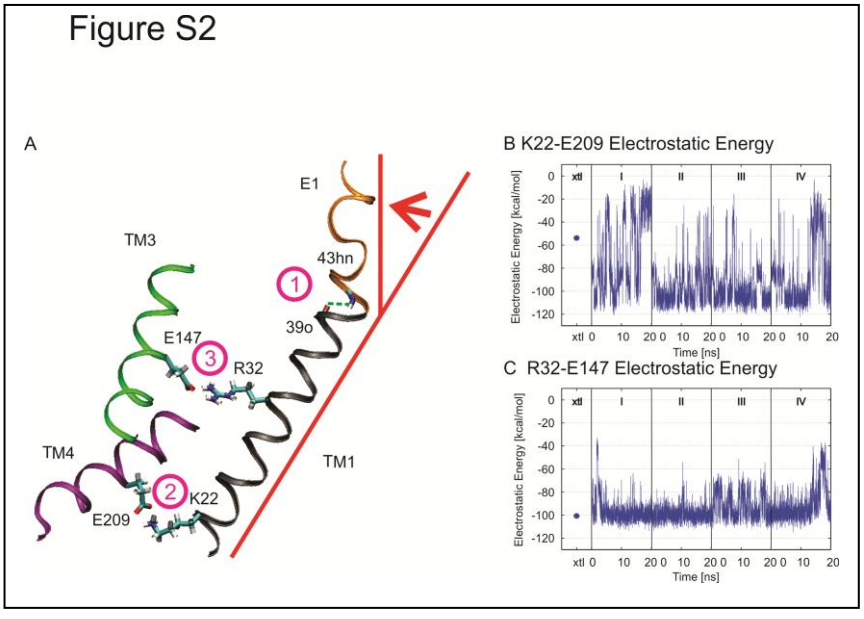

8. Figure S3. Time series of properties indicated in Fig. 4 for the entire MD simulations, including the 140 ns equilibration and 4 – 20 ns production stage simulations. The time series behaviors were asynchronous over the first 100 ns of the production stage simulation and several time series properties were not equilibrated prior to 100 ns. At ~ 100 ns, fluctuations among the time series of indicated properties became synchronized, fluctuating in unison for the remainder of the equilibration stage (100-140 ns: green bar) and throughout the 4 – 20 ns production stage simulations (see Fig S4 below).

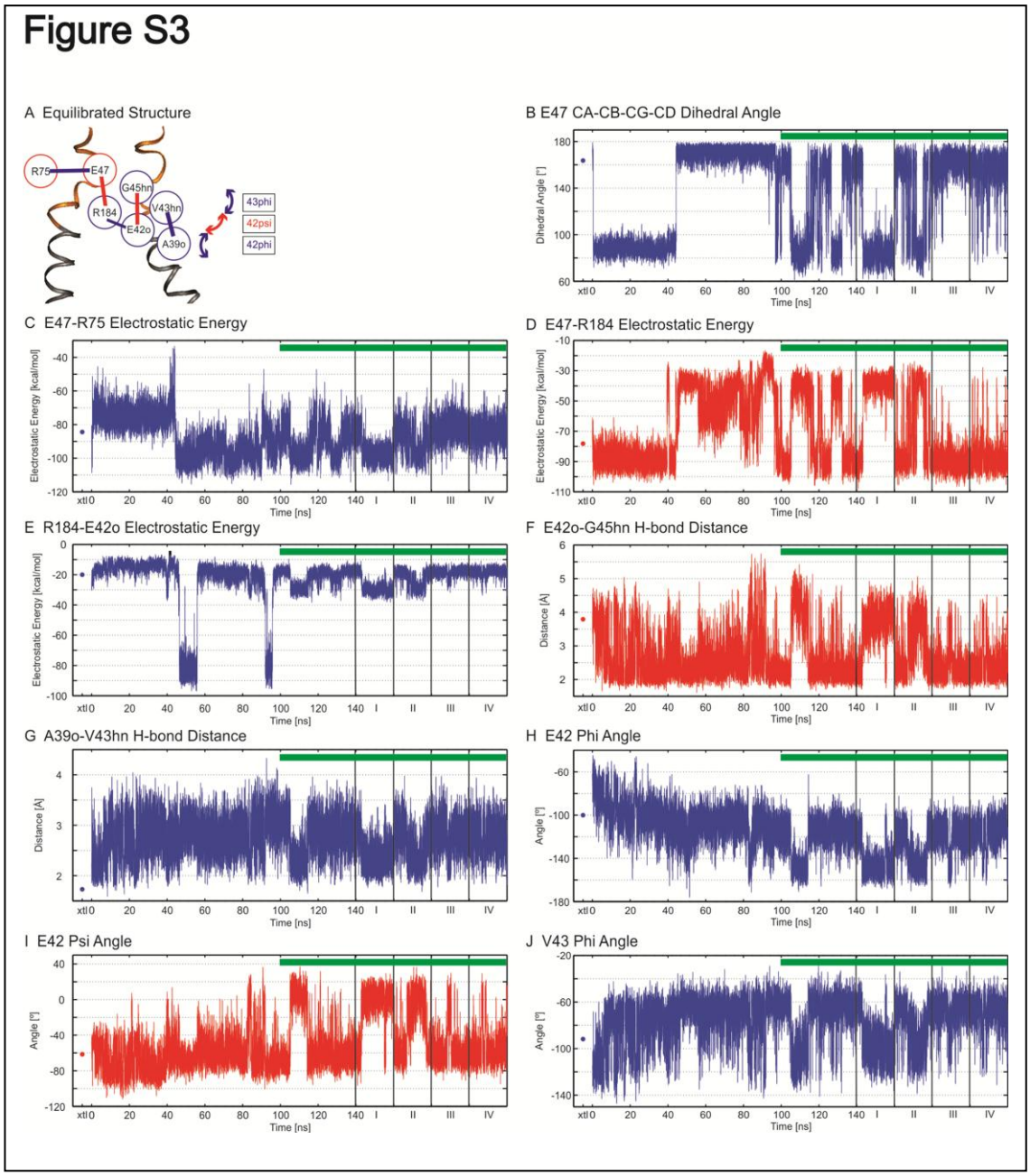

9. Figure S4. Cross-correlations between the time series of properties presented in Fig. 4. Cross-correlations are shown for properties of adjacent residues shown in Panel A. Panel B is a control – cross-correlation analysis was performed on time series E47 dihedral angle x E47 dihedral angle to illustrate the plot of a perfect correlated time series. The cross correlation relation of this comparison is centered at a lag-time (delay) of 0 and

the correlation-time lag relation is perfectly symmetric. The time delay is the lag-time at maximum correlation. A time delay of 0 means that the two time series are synchronized at t = 0; perfect symmetry means that the two time series are synchronized over the entire time series. The degree of asymmetry in the cross-correlation - time lag relation was determined with the equation:

$$Asymmetry = \sum_{t=0}^{4000}(correlation\ (t) - correlation(-t))^2 : [t] = 0.01\ ns$$

All cross-correlations of the time series properties were centered at a time-lag of 0 with correlations > 0.70 at this value and displayed a high degree of symmetry; indicating highly synchronous behavior of the time series properties compared.

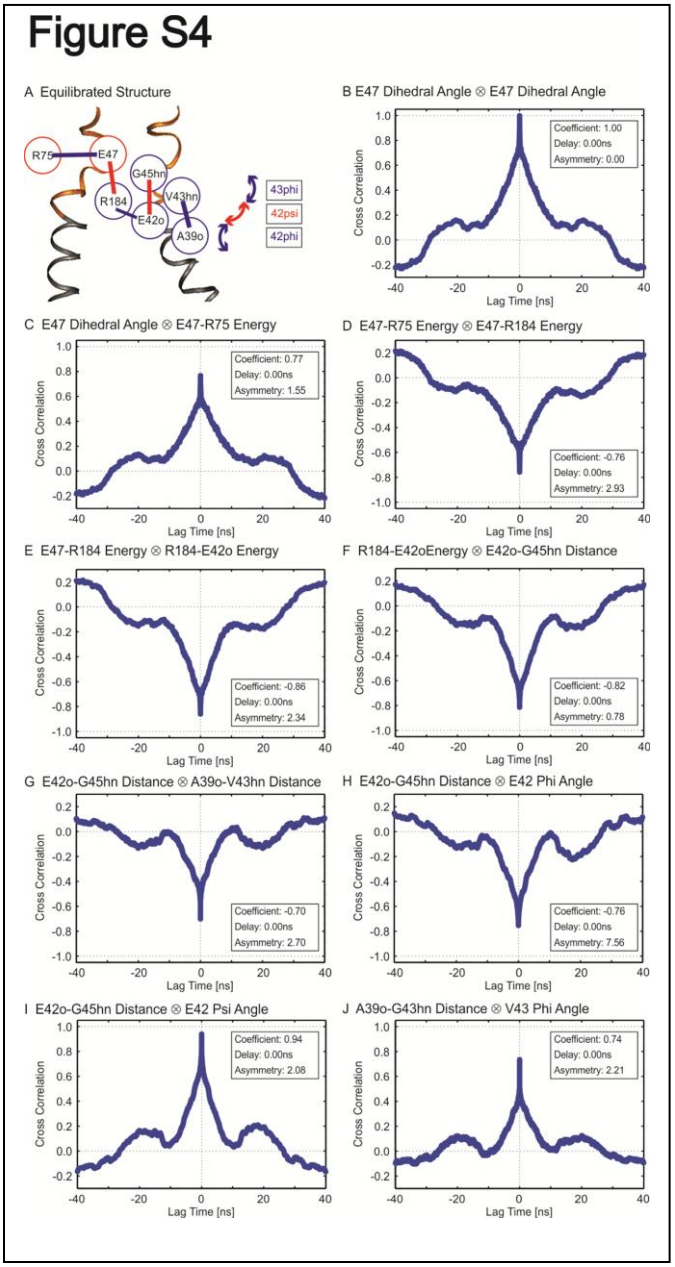

10. Figure S5. Schematic illustration of the intracellular portion of the channel pore showing the proposed formation of the loop-gate permeability barrier by change in structure of the parahelix that allows it to protrude into the channel pore (1) and straightening of the TM1/E1 bend angle which reduces the pore diameter at the cytoplasmic entrance of the channel pore. Parahelix is depicted in red; TM1-blue; NT residues 1-15 - green, and the cytoplasmic portion (residues 87-108) of TM2 yellow.

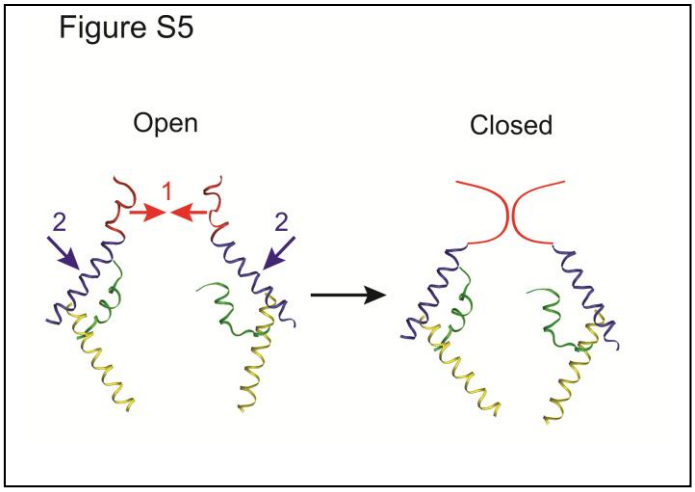

Table S1. vdW interaction energies of residues pairs: blue – intra-subunit, red inter-subunit interactions.

A. Crystal structure

	35	36	38	39	40	43	44	51	65	68	69	71	74	76	77	79	154	158	163	182	191	195	196	191
35	x	x	x	x	x	x	x	x	x	x	x	x	x	x	x	x	x	x	x	x	-0.85	x	x	x
36	x	x	x	x	x	x	x	x	x	x	x	x	-0.64	x	1.76	x	x	x	x	x	x	-0.30	x	x
38	x	x	x	x	x	x	x	x	x	x	x	x	x	x	x	x	x	x	x	x	1.66	x	x	x
39	x	x	x	x	x	x	-0.42	x	x	x	x	x	-0.44	x	x	x	x	x	x	x	5.40	-0.11	x	x
40	x	x	x	x	x	x	x	x	x	x	x	x	0.82	x	x	x	x	x	x	x	x	x	x	x
43	x	x	x	x	x	x	3.04	x	x	x	x	x	x	x	x	x	x	x	x	x	-0.63	x	x	x
44	x	x	x	-0.42	x	3.04	x	x	x	x	-0.65	x	-2.34	x	x	x	x	x	0.17	x	x	x	x	x
51	x	x	x	x	x	x	x	x	-1.62	x	x	x	x	x	x	x	x	x	x	x	x	x	x	x
65	x	x	x	x	x	x	x	-1.62	x	x	-2.45	x	x	x	x	x	x	x	x	x	x	x	x	x
68	x	x	x	x	x	x	x	x	x	x	0.07	x	x	x	x	x	x	x	-0.03	x	x	x	x	x
69	x	x	x	x	x	x	-0.65	x	-2.45	0.07	x	x	x	x	x	x	x	-0.81	x	-1.00	x	x	x	x
71	x	x	x	x	x	x	x	x	x	x	x	x	x	x	x	x	x	x	x	x	x	x	x	-0.76
74	x	-0.64	x	-0.44	0.82	x	-2.34	x	x	x	x	x	x	x	2.10	x	x	x	x	x	x	-0.23	x	x
76	x	x	x	x	x	x	x	x	x	x	x	x	x	x	x	x	4.34	x	x	x	x	x	x	x
77	x	1.76	x	x	x	x	x	x	x	x	x	x	2.10	x	x	x	-3.39	x	x	x	x	-1.51	1.27	x
79	x	x	x	x	x	x	x	x	x	x	x	x	x	x	x	x	x	x	x	x	x	x	x	-0.98
154	x	x	x	x	x	x	x	x	x	x	x	x	x	4.34	-3.39	x	x	x	x	x	x	x	x	x
158	x	x	x	x	x	x	x	x	x	x	-0.81	x	x	x	x	x	x	x	x	x	x	x	x	x
163	x	x	x	x	x	x	0.17	x	x	-0.03	x	x	x	x	x	x	x	x	x	-0.81	x	x	x	x
182	x	x	x	x	x	x	x	x	x	x	-1.00	x	x	x	x	x	x	x	-0.81	x	x	x	x	x
191	-0.85	x	1.66	5.40	x	-0.63	x	x	x	x	x	x	x	x	x	x	x	x	x	x	x	x	x	x
195	x	-0.30	x	-0.11	x	x	x	x	x	x	x	x	-0.23	x	-1.51	x	x	x	x	x	x	x	x	x
196	x	x	x	x	x	x	x	x	x	x	x	x	x	x	1.27	x	x	x	x	x	x	x	x	x
191	x	x	x	x	x	x	x	x	x	x	x	-0.76	x	x	x	-0.98	x	x	x	x	x	x	x	x

B. Equilibrated structure (WT)

	35	36	38	39	40	43	44	51	65	68	69	71	74	76	77	79	154	158	163	182	191	195	196	*191
35	x	x	x	x	x	x	x	x	x	x	x	x	x	x	x	x	x	x	x	x	-0.82	x	x	x
36	x	x	x	x	x	x	x	x	x	x	x	x	-0.52	x	-0.64	x	x	x	x	x	x	-0.99	x	x
38	x	x	x	x	x	x	x	x	x	x	x	x	x	x	x	x	x	x	x	x	-0.80	x	x	x
39	x	x	x	x	x	-0.27	-0.33	x	x	x	x	x	-0.30	x	x	x	x	x	x	x	-0.48	-0.18	x	x
40	x	x	x	x	x	x	-0.09	x	x	x	x	x	-0.35	x	x	x	x	x	x	x	x	x	x	x
43	x	x	x	-0.27	x	x	-0.90	x	x	x	x	x	x	x	x	x	x	x	x	x	-1.25	x	x	x
44	x	x	x	-0.33	-0.09	-0.90	x	x	x	x	-0.62	x	-1.69	x	x	x	x	x	-1.20	x	x	x	x	x
51	x	x	x	x	x	x	x	x	-1.81	x	x	x	x	x	x	x	x	x	x	x	x	x	x	x
65	x	x	x	x	x	x	x	-1.81	x	x	-2.00	x	x	x	x	x	x	x	x	x	x	x	x	x
68	x	x	x	x	x	x	x	x	x	x	-1.92	x	x	x	x	x	x	x	-0.37	x	x	x	x	x
69	x	x	x	x	x	x	-0.62	x	-2.00	-1.92	x	x	x	x	x	x	x	-1.02	x	-0.34	x	x	x	x
71	x	x	x	x	x	x	x	x	x	x	x	x	x	x	x	x	x	x	x	x	x	x	x	-0.67
74	x	-0.52	x	-0.30	-0.35	x	-1.69	x	x	x		x	x	x	-0.71	x	x	x	x	x	x	-0.53	x	x
76	x	x	x	x	x	x	x	x	x	x	x	x	x	x	x	x	-0.78	x	x	x	x	x	x	x
77	x	-0.64	x	x	x	x	x	x	x	x	x	x	-0.71	x	x	x	-2.30	x	x	x	x	-2.55	-0.80	x
79	x	x	x	x	x	x	x	x	x	x	x	x	x	x	x	x	x	x	x	x	x	x	x	-1.07
154	x	x	x	x	x	x	x	x	x	x	x	x	x	-0.78	-2.30	x	x	x	x	x	x	x	x	x
158	x	x	x	x	x	x	x	x	x	x	-1.02	x	x	x	x	x	x	x	x	x	x	x	x	x
163	x	x	x	x	x	x	-1.20	x	x	-0.37	x	x	x	x	x	x	x	x	x	-0.61	x	x	x	x
182	x	x	x	x	x	x	x	x	x	x	-0.34	x	x	x	x	x	x	x	-0.61	x	x	x	x	x
191	-0.82	x	-0.80	-0.48	x	-1.25	x	x	x	x	x	x	x	x	x	x	x	x	x	x	x	x	x	x
195	x	-0.99	x	-0.18	x	x	x	x	x	x	x	x	-0.53	x	-2.55	x	x	x	x	x	x	x	x	x
196	x	x	x	x	x	x	x	x	x	x	x	x	x	x	-0.80	x	x	x	x	x	x	x	x	x
*191	x	x	x	x	x	x	x	x	x	x	x	-0.67	x	x	x	-1.07	x	x	x	x	x	x	x	x

Residue pairs shaded red were identified in the cluster analysis (MMTSB) but these were excluded from the interaction list by the criteria used in the construction of interaction lists described above. The calculated average energies for all pairs of residues in the final interaction list were < - 0.34 kcal/mol.

C. V43A+I74V

	35	36	38	39	40	43	44	51	65	68	69	71	74	76	77	79	154	158	163	182	191	195	196	*191
35	x	x	x	x	x	x	x	x	x	x	x	x	x	x	x	x	x	x	x	x	-0.78	x	x	x
36	x	x	x	x	x	x	x	x	x	x	x	x	-0.41	x	-0.74	x	x	x	x	x	x	-1.05	x	x
38	x	x	x	x	x	x	x	x	x	x	x	x	x	x	x	x	x	x	x	x	-0.84	x	x	x
39	x	x	x	x	x	x	-0.36	x	x	x	x	x	-0.27	x	x	x	x	x	x	x	-0.44	-0.24	x	x
40	x	x	x	x	x	x	x	x	x	x	x	x	-0.33	x	x	x	x	x	x	x	x	x	x	x
43	x	x	x	x	x	x	-0.48	x	x	x	x	x	x	x	x	x	x	x	x	x	-0.60	x	x	x
44	x	x	x	-0.36	x	-0.48	x	x	x	x	-0.63	x	-1.46	x	x	x	x	x	-1.25	x	x	x	x	x
51	x	x	x	x	x	x	x	x	-1.81	x	x	x	x	x	x	x	x	x	x	x	x	x	x	x
65	x	x	x	x	x	x	x	-1.81	x	x	-2.04	x	x	x	x	x	x	x	x	x	x	x	x	x
68	x	x	x	x	x	x	x	x	x	x	-1.80	x	x	x	x	x	x	x	-0.32	x	x	x	x	x
69	x	x	x	x	x	x	-0.63	x	-2.04	-1.80	x	x	x	x	x	x	x	-0.96	x	-0.38	x	x	x	x
71	x	x	x	x	x	x	x	x	x	x	x	x	x	x	x	x	x	x	x	x	x	x	x	-0.69
74	x	-0.41	x	-0.27	-0.33	x	-1.46	x	x	x	x	x	x	x	-0.40	x	x	x	x	x	x	-0.27	x	x
76	x	x	x	x	x	x	x	x	x	x	x	x	x	x	x	x	-0.77	x	x	x	x	x	x	x
77	x	-0.74	x	x	x	x	x	x	x	x	x	x	-0.40	x	x	x	-2.31	x	x	x	x	-2.57	-0.77	x
79	x	x	x	x	x	x	x	x	x	x	x	x	x	x	x	x	x	x	x	x	x	x	x	-0.98
154	x	x	x	x	x	x	x	x	x	x	x	x	x	-0.77	-2.31	x	x	x	x	x	x	x	x	x
158	x	x	x	x	x	x	x	x	x	x	-0.96	x	x	x	x	x	x	x	x	x	x	x	x	x
163	x	x	x	x	x	x	-1.25	x	x	-0.32	x	x	x	x	x	x	x	x	x	-0.59	x	x	x	x	x
182	x	x	x	x	x	x	x	x	x	x	-0.38	x	x	x	x	x	x	x	-0.59	x	x	x	x	x
191	-0.78	x	-0.84	-0.44	x	-0.60	x	x	x	x	x	x	x	x	x	x	x	x	x	x	x	x	x	x
195	x	-1.05	x	-0.24	x	x	x	x	x	x	x	x	-0.27	x	-2.57	x	x	x	x	x	x	x	x	x
196	x	x	x	x	x	x	x	x	x	x	x	x	x	x	-0.77	x	x	x	x	x	x	x	x	x
*191	x	x	x	x	x	x	x	x	x	x	x	-0.69	x	x	x	-0.98	x	x	x	x	x	x	x	x

Table S2. Electrostatic interaction energies of residue pairs: blue – intra-subunit, red inter-subunit interactions.

A. Crystal structure

	22	32	42	46	47	48	50	62	66	75	80	139	143	147	183	184	187	188	199	206	209	46	48	62	65	72	75	165	184	186
22	x	x	x	x	x	x	x	x	x	x	x	x	x	x	x	x	x	x	x	x	-53.46	x	x	x	x	x	x	x	x	x
32	x	x	x	x	x	x	x	x	x	x	-7.52	x	x	-83.54	x	x	x	x	-8.13	x	x	x	x	x	x	x	x	x	x	x
42	x	x	x	x	x	x	x	x	x	x	x	x	x	x	x	-18.13	x	x	x	x	x	x	x	x	x	x	-46.21	x	x	x
46	x	x	x	x	x	x	x	x	x	x	x	x	x	x	x	-60.67	x	-15.88	x	x	x	x	-20.94	x	x	x	x	x	x	x
47	x	x	x	x	x	x	x	x	x	-83.88	x	x	x	x	x	x	x	x	x	x	x	x	x	x	x	x	x	x	-76.63	x
48	x	x	x	x	x	x	x	1.60	x	x	x	x	x	x	x	x	x	x	x	x	x	x	x	x	x	x	x	x	x	x
50	x	x	x	x	x	x	x	x	x	x	x	x	x	x	x	x	x	x	x	x	x	x	-10.85	-2.09	x	x	x	x	x	x
62	x	x	x	x	x	1.60	x	x	x	x	x	x	x	x	x	x	x	x	x	x	x	x	x	x	x	x	x	x	x	x
66	x	x	x	x	x	x	x	x	x	x	x	x	x	x	x	x	x	x	x	x	x	x	x	x	x	x	x	-40.40	x	-33.87
75	x	x	x	x	-83.88	x	x	x	x	x	x	x	x	x	x	x	x	x	x	x	x	x	x	x	x	x	x	x	x	x
80	x	-7.52	x	x	x	x	x	x	x	x	x	x	x	x	x	x	x	x	x	x	x	x	x	x	x	x	x	x	x	x
139	x	x	x	x	x	x	x	x	x	x	x	x	-17.32	x	x	x	x	x	x	x	x	x	x	x	x	x	x	x	x	x
143	x	x	x	x	x	x	x	x	x	x	x	-17.32		-3.66	x	x	x	x	x	-14.95	-3.66	x	x	x	x	x	x	x	x	x
147	x	-83.54	x	x	x	x	x	x	x	x	x	x	-3.66	x	x	x	x	x	x	x	x	x	x	x	x	x	x	x	x	x
183	x	x	x	x	x	x	x	x	x	x	x	x	x	x	x	x	x	x	x	x	x	x	2.17	x	x	x	x	x	x	x
184	x	x	-18.13	-60.67	x	x	x	x	x	x	x	x	x	x	x	x	x	x	x	x	x	x	x	x	3.21	x	x	x	x	x
187	x	x	x	x	x	x	x	x	x	x	x	x	x	x	x	x	x	x	x	x	x	x	x	x	x	-8.21	-88.92	x	x	x
188	x	x	x	-15.88	x	x	x	x	x	x	x	x	x	x	x	x	x	x	x	x	x	x	x	x	x	x	x	x	x	x
199	x	-8.13	x	x	x	x	x	x	x	x	x	x	x	x	x	x	x	x	x	x	x	x	x	x	x	x	x	x	x	x
206	x	x	x	x	x	x	x	x	x	x	x	x	-14.95	x	x	x	x	x	x	x	x	x	x	x	x	x	x	x	x	x
209	-53.46	x	x	x	x	x	x	x	x	x	x	x	-3.66	x	x	x	x	x	x	x	x	x	x	x	x	x	x	x	x	x
46	x	x	x	x	x	x	x	x	x	x	x	x	x	x	x	x	x	x	x	x	x	x	x	x	x	x	x	x	x	x
48	x	x	x	-20.94	x	x	-10.85	x	x	x	x	x	x	x	2.17	x	x	x	x	x	x	x	x	x	x	x	x	x	x	x
62	x	x	x	x	x	x	-2.09	x	x	x	x	x	x	x	x	x	x	x	x	x	x	x	x	x	x	x	x	x	x	x
65	x	x	x	x	x	x	x	x	x	x	x	x	x	x	x	3.21	x	x	x	x	x	x	x	x	x	x	x	x	x	x
72	x	x	x	x	x	x	x	x	x	x	x	x	x	x	x	x	-8.21	x	x	x	x	x	x	x	x	x	x	x	x	x
75	x	x	-46.21	x	x	x	x	x	x	x	x	x	x	x	x	x	-88.92	x	x	x	x	x	x	x	x	x	x	x	x	x
165	x	x	x	x	x	x	x	x	-40.40	x	x	x	x	x	x	x	x	x	x	x	x	x	x	x	x	x	x	x	x	x
184	x	x	x	x	-76.63	x	x	x	x	x	x	x	x	x	x	x	x	x	x	x	x	x	x	x	x	x	x	x	x	x
186	x	x	x	x	x	x	x	x	-33.87	x	x	x	x	x	x	x	x	x	x	x	x	x	x	x	x	x	x	x	x	x

B. Equilibrated structure (WT)

	22	32	42	46	47	48	50	62	66	75	80	139	143	147	183	184	187	188	199	206	209	46	48	62	65	72	75	165	184	186
22	x	x	x	x	x	x	x	x	x	x	x	x	x	x	x	x	x	x	x	x	-90.21	x	x	x	x	x	x	x	x	x
32	x	x	x	x	x	x	x	x	x	x	0.03	x	x	-98.53	x	x	x	x	-9.99	x	x	x	x	x	x	x	x	x	x	x
42	x	x	x	x	x	x	x	x	x	x	x	x	x	x	x	-25.49	x	x	x	x	x	x	x	x	x	x	-75.11	x	x	x
46	x	x	x	x	x	x	x	x	x	x	x	x	x	x	x	-60.83	x	-65.85	x	x	x	x	-4.50	x	x	x	x	x	x	x
47	x	x	x	x	x	x	x	x	x	-92.02	x	x	x	x	x	x	x	x	x	x	x	x	x	x	x	x	x	x	-51.47	x
48	x	x	x	x	x	x	x	-0.23	x	x	x	x	x	x	x	x	x	x	x	x	x	x	x	x	x	x	x	x	x	x
50	x	x	x	x	x	x	x	x	x	x	x	x	x	x	x	x	x	x	x	x	x	x	-3.33	-1.92	x	x	x	x	x	x
62	x	x	x	x	x	-0.23	x	x	x	x	x	x	x	x	x	x	x	x	x	x	x	x	x	x	x	x	x	x	x	x
66	x	x	x	x	x	x	x	x	x	x	x	x	x	x	x	x	x	x	x	x	x	x	x	x	x	x	x	-67.06	x	-30.61
75	x	x	x	x	-92.02	x	x	x	x	x	x	x	x	x	x	x	x	x	x	x	x	x	x	x	x	x	x	x	x	x
80	x	0.03	x	x	x	x	x	x	x	x	x	x	x	x	x	x	x	x	x	x	x	x	x	x	x	x	x	x	x	x
139	x	x	x	x	x	x	x	x	x	x	x	x	-7.56	x	x	x	x	x	x	x	x	x	x	x	x	x	x	x	x	x
143	x	x	x	x	x	x	x	x	x	x	x	-7.56		-26.83	x	x	x	x	x	-6.34	-29.14	x	x	x	x	x	x	x	x	x
147	x	-98.53	x	x	x	x	x	x	x	x	x	x	-26.83	x	x	x	x	x	x	x	x	x	x	x	x	x	x	x	x	x
183	x	x	x	x	x	x	x	x	x	x	x	x	x	x	x	x	x	x	x	x	x	x	-1.96	x	x	x	x	x	x	x
184	x	x	-25.49	-60.83	x	x	x	x	x	x	x	x	x	x	x	x	x	x	x	x	x	x	x	x	4.47	x	x	x	x	x
187	x	x	x	x	x	x	x	x	x	x	x	x	x	x	x	x	x	x	x	x	x	x	x	x	x	-17.99	-80.60	x	x	x
188	x	x	x	-65.85	x	x	x	x	x	x	x	x	x	x	x	x	x	x	x	x	x	x	x	x	x	x	x	x	x	x
199	x	-9.99	x	x	x	x	x	x	x	x	x	x	x	x	x	x	x	x	x	x	x	x	x	x	x	x	x	x	x	x
206	x	x	x	x	x	x	x	x	x	x	x	x	-6.34	x	x	x	x	x	x	x	x	x	x	x	x	x	x	x	x	x
209	-90.21	x	x	x	x	x	x	x	x	x	x	x	-29.14	x	x	x	x	x	x	x	x	x	x	x	x	x	x	x	x	x
46	x	x	x	x	x	x	x	x	x	x	x	x	x	x	x	x	x	x	x	x	x	x	x	x	x	x	x	x	x	x
48	x	x	x	-4.50	x	x	-3.33	x	x	x	x	x	x	x	-1.96	x	x	x	x	x	x	x	x	x	x	x	x	x	x	x
62	x	x	x	x	x	x	-1.92	x	x	x	x	x	x	x	x	x	x	x	x	x	x	x	x	x	x	x	x	x	x	x
65	x	x	x	x	x	x	x	x	x	x	x	x	x	x	x	4.47	x	x	x	x	x	x	x	x	x	x	x	x	x	x
72	x	x	x	x	x	x	x	x	x	x	x	x	x	x	x	x	-17.99	x	x	x	x	x	x	x	x	x	x	x	x	x
75	x	x	-75.11	x	x	x	x	x	x	x	x	x	x	x	x	x	-80.60	x	x	x	x	x	x	x	x	x	x	x	x	x
165	x	x	x	x	x	x	x	x	-67.06	x	x	x	x	x	x	x	x	x	x	x	x	x	x	x	x	x	x	x	x	x
184	x	x	x	x	-51.47	x	x	x	x	x	x	x	x	x	x	x	x	x	x	x	x	x	x	x	x	x	x	x	x	x
186	x	x	x	x	x	x	x	x	-30.61	x	x	x	x	x	x	x	x	x	x	x	x	x	x	x	x	x	x	x	x	x

C. V43A+I74V

	22	32	42	46	47	48	50	62	66	75	80	139	143	147	183	184	187	188	199	206	209	46	48	62	65	72	75	165	184	186
22	x	x	x	x	x	x	x	x	x	x	x	x	x	x	x	x	x	x	x	x	-93.02	x	x	x	x	x	x	x	x	x
32	x	x	x	x	x	x	x	x	x	x	0.05	x	x	-99.60	x	x	x	x	-10.53	x	x	x	x	x	x	x	x	x	x	x
42	x	x	x	x	x	x	x	x	x	x	x	x	x	x	x	-25.74	x	x	x	x	x	x	x	x	x	x	-77.03	x	x	x
46	x	x	x	x	x	x	x	x	x	x	x	x	x	x	x	-61.93	x	-66.31	x	x	x	x	-4.05	x	x	x	x	x	x	x
47	x	x	x	x	x	x	x	x	x	-92.36	x	x	x	x	x	x	x	x	x	x	x	x	x	x	x	x	x	x	-47.73	x
48	x	x	x	x	x	x	x	-0.23	x	x	x	x	x	x	x	x	x	x	x	x	x	x	x	x	x	x	x	x	x	x
50	x	x	x	x	x	x	x	x	x	x	x	x	x	x	x	x	x	x	x	x	x	x	-2.89	-1.78	x	x	x	x	x	x
62	x	x	x	x	x	-0.23	x	x	x	x	x	x	x	x	x	x	x	x	x	x	x	x	x	x	x	x	x	x	x	x
66	x	x	x	x	x	x	x	x	x	x	x	x	x	x	x	x	x	x	x	x	x	x	x	x	x	x	x	-66.04	x	-30.46
75	x	x	x	-92.36	x	x	x	x	x	x	x	x	x	x	x	x	x	x	x	x	x	x	x	x	x	x	x	x	x	x
80	x	0.05	x	x	x	x	x	x	x	x	x	x	x	x	x	x	x	x	x	x	x	x	x	x	x	x	x	x	x	x
139	x	x	x	x	x	x	x	x	x	x	x	x	-7.22	x	x	x	x	x	x	x	x	x	x	x	x	x	x	x	x	x
143	x	x	x	x	x	x	x	x	x	x	x	-7.22		-27.36	x	x	x	x	x	-6.82	-29.30	x	x	x	x	x	x	x	x	x
147	x	-99.60	x	x	x	x	x	x	x	x	x	x	-27.36	x	x	x	x	x	x	x	x	x	x	x	x	x	x	x	x	x
183	x	x	x	x	x	x	x	x	x	x	x	x	x	x	x	x	x	x	x	x	x	x	-1.98	x	x	x	x	x	x	x
184	x	x	-25.74	-61.93	x	x	x	x	x	x	x	x	x	x	x	x	x	x	x	x	x	x	x	x	4.65	x	x	x	x	x
187	x	x	x	x	x	x	x	x	x	x	x	x	x	x	x	x	x	x	x	x	x	x	x	x	x	-17.33	-80.90	x	x	x
188	x	x	x	-66.31	x	x	x	x	x	x	x	x	x	x	x	x	x	x	x	x	x	x	x	x	x	x	x	x	x	x
199	x	-10.53	x	x	x	x	x	x	x	x	x	x	x	x	x	x	x	x	x	x	x	x	x	x	x	x	x	x	x	x
206	x	x	x	x	x	x	x	x	x	x	x	x	-6.82	x	x	x	x	x	x	x	x	x	x	x	x	x	x	x	x	x
209	-93.02	x	x	x	x	x	x	x	x	x	x	x	-29.30	x	x	x	x	x	x	x	x	x	x	x	x	x	x	x	x	x
46	x	x	x	x	x	x	x	x	x	x	x	x	x	x	x	x	x	x	x	x	x	x	x	x	x	x	x	x	x	x
48	x	x	x	-4.05	x	x	-2.89	x	x	x	x	x	x	x	-1.98	x	x	x	x	x	x	x	x	x	x	x	x	x	x	x
62	x	x	x	x	x	x	-1.78	x	x	x	x	x	x	x	x	x	x	x	x	x	x	x	x	x	x	x	x	x	x	x
65	x	x	x	x	x	x	x	x	x	x	x	x	x	x	x	4.65	x	x	x	x	x	x	x	x	x	x	x	x	x	x
72	x	x	x	x	x	x	x	x	x	x	x	x	x	x	x	x	-17.33	x	x	x	x	x	x	x	x	x	x	x	x	x
75	x	x	-77.03	x	x	x	x	x	x	x	x	x	x	x	x	x	-80.90	x	x	x	x	x	x	x	x	x	x	x	x	x
165	x	x	x	x	x	x	x	x	-66.04	x	x	x	x	x	x	x	x	x	x	x	x	x	x	x	x	x	x	x	x	x
184	x	x	x	x	-47.73	x	x	x	x	x	x	x	x	x	x	x	x	x	x	x	x	x	x	x	x	x	x	x	x	x
186	x	x	x	x	x	x	x	x	-30.46	x	x	x	x	x	x	x	x	x	x	x	x	x	x	x	x	x	x	x	x	x

REFERENCES

1. Maeda, S., S. Nakagawa, M. Suga, E. Yamashita, A. Oshima, Y. Fujiyoshi, and T. Tsukihara. 2009. Structure of the connexin 26 gap junction channel at 3.5 A resolution. Nature 458:597-602.
2. Purnick, P. E., D. C. Benjamin, V. K. Verselis, T. A. Bargiello, and T. L. Dowd. 2000. Structure of the amino terminus of a gap junction protein. Archives of biochemistry and biophysics 381:181-190.
3. Ishida, T., and K. Kinoshita. 2007. PrDOS: prediction of disordered protein regions from amino acid sequence. Nucleic Acids Research 35:W460-W464.
4. MacKerell, A. D., D. Bashford, M. Bellott, R. L. Dunbrack, J. D. Evanseck, M. J. Field, S. Fischer, J. Gao, H. Guo, S. Ha, D. Joseph-McCarthy, L. Kuchnir, K. Kuczera, F. T. K. Lau, C. Mattos, S. Michnick, T. Ngo, D. T. Nguyen, B. Prodhom, W. E. Reiher, B. Roux, M. Schlenkrich, J. C. Smith, R. Stote, J. Straub, M. Watanabe, J. Wiorkiewicz-Kuczera, D. Yin, and M. Karplus. 1998. All-atom empirical potential for molecular modeling and dynamics studies of proteins. Journal of Physical Chemistry B 102:3586-3616.
5. Mackerell, A. D. 2004. Empirical force fields for biological macromolecules: Overview and issues. Journal of Computational Chemistry 25:1584-1604.
6. Li, H., A. D. Robertson, and J. H. Jensen. 2005. Very fast empirical prediction and rationalization of protein pKa values. Proteins: Structure, Function, and Bioinformatics 61:704-721.
7. Bas, D. C., D. M. Rogers, and J. H. Jensen. 2008. Very fast prediction and rationalization of pKa values for protein–ligand complexes. Proteins: Structure, Function, and Bioinformatics 73:765-783.
8. Olsson, M. H. M., C. R. Søndergaard, M. Rostkowski, and J. H. Jensen. 2011. PROPKA3: Consistent Treatment of Internal and Surface Residues in Empirical pKa Predictions. Journal of Chemical Theory and Computation 7:525-537.
9. Eldho, N. V., S. E. Feller, S. Tristram-Nagle, I. V. Polozov, and K. Gawrisch. 2003. Polyunsaturated Docosahexaenoic vs Docosapentaenoic AcidDifferences in Lipid Matrix Properties from the Loss of One Double Bond. Journal of the American Chemical Society 125:6409-6421.
10. Jo, S., T. Kim, and W. Im. 2007. Automated builder and database of protein/membrane complexes for molecular dynamics simulations. PloS one 2:e880.
11. Jo, S., T. Kim, V. G. Iyer, and W. Im. 2008. CHARMM-GUI: a web-based graphical user interface for CHARMM. Journal of computational chemistry 29:1859-1865.
12. Jo, S., J. B. Lim, J. B. Klauda, and W. Im. 2009. CHARMM-GUI Membrane Builder for mixed bilayers and its application to yeast membranes. Biophys J 97:50-58.

13. Mackerell, A. D., Jr., M. Feig, and C. L. Brooks, 3rd. 2004. Extending the treatment of backbone energetics in protein force fields: limitations of gas-phase quantum mechanics in reproducing protein conformational distributions in molecular dynamics simulations. Journal of computational chemistry 25:1400-1415.
14. Klauda, J. B., B. R. Brooks, A. D. MacKerell, R. M. Venable, and R. W. Pastor. 2005. An ab Initio Study on the Torsional Surface of Alkanes and Its Effect on Molecular Simulations of Alkanes and a DPPC Bilayer. The Journal of Physical Chemistry B 109:5300-5311.
15. Brooks, B. R., R. E. Bruccoleri, B. D. Olafson, D. J. States, S. Swaminathan, and M. Karplus. 1983. CHARMM: A Program for Macromolecular Energy, Minimization, and Dynamics Calculations. Journal of computational chemistry 4:187-217.
16. Brooks, B. R., C. L. Brooks, 3rd, A. D. Mackerell, Jr., L. Nilsson, R. J. Petrella, B. Roux, Y. Won, G. Archontis, C. Bartels, S. Boresch, A. Caflisch, L. Caves, Q. Cui, A. R. Dinner, M. Feig, S. Fischer, J. Gao, M. Hodoscek, W. Im, K. Kuczera, T. Lazaridis, J. Ma, V. Ovchinnikov, E. Paci, R. W. Pastor, C. B. Post, J. Z. Pu, M. Schaefer, B. Tidor, R. M. Venable, H. L. Woodcock, X. Wu, W. Yang, D. M. York, and M. Karplus. 2009. CHARMM: the biomolecular simulation program. Journal of computational chemistry 30:1545-1614.
17. Woolf, T. B., and B. Roux. 1994. Molecular dynamics simulation of the gramicidin channel in a phospholipid bilayer. Proc Natl Acad Sci U S A 91:11631-11635.
18. Woolf, T. B., and B. Roux. 1996. Structure, energetics, and dynamics of lipid-protein interactions: A molecular dynamics study of the gramicidin A channel in a DMPC bilayer. Proteins 24:92-114.
19. Hoover, W. G. 1985. Canonical dynamics: Equilibrium phase-space distributions. Physical review. A 31:1695-1697.
20. Phillips, J. C., R. Braun, W. Wang, J. Gumbart, E. Tajkhorshid, E. Villa, C. Chipot, R. D. Skeel, L. Kale, and K. Schulten. 2005. Scalable molecular dynamics with NAMD. Journal of computational chemistry 26:1781-1802.
21. Essmann, U., L. Perera, M. L. Berkowitz, T. Darden, H. Lee, and L. G. Pedersen. 1995. A Smooth Particle Mesh Ewald Method. J. Chem. Phys. 103:8577-8593.
22. Kwon, T., A. L. Harris, A. Rossi, and T. A. Bargiello. 2011. Molecular dynamics simulations of the Cx26 hemichannel: Evaluation of structural models with Brownian dynamics. J Gen Physiol 138:475-493.
23. Enkhbayar, P., K. Hikichi, M. Osaki, R. H. Kretsinger, and N. Matsushima. 2006. 3_{10}-helices in proteins are parahelices. Proteins: Structure, Function, and Bioinformatics 64:691-699.
24. De Loof, H., L. Nilsson, and R. Rigler. 1992. Molecular dynamics simulation of galanin in aqueous and nonaqueous solution. Journal of the American Chemical Society 114:4028-4035.